Struct Multidisc Optim (2008) 36:307–317
DOI 10.1007/s00158-007-0166-7

RESEARCH PAPER

Structural dynamic shape optimization and sensitivity analysis based on RKPM

Jianping Zhang · Shuguang Gong · Yunqing Huang · Aihong Qiu · Renke Chen

Received: 9 February 2007 / Revised: 29 May 2007 / Accepted: 18 July 2007 / Published online: 22 September 2007

Abstract A numerical method of structural dynamic shape optimization is presented by using reproducing kernel particle method (RKPM), by which the mesh distortion that exists in shape optimal method based on finite element can be eliminated completely and the optimal model for structural dynamic optimization design is built. The discreteness-based design sensitivity analysis in both natural frequency and dynamic response is proposed by using direct differentiation method and discrete derivatives on the basis of structural dynamic analysis, in which the penalty method is employed into imposing the essential boundary conditions, and the derivatives of shape functions with respect to design variables are derived. The algorithm of dynamic sensitivity analysis is testified by numerical example, and the numerical results obtained are in good agreement with those obtained using semi-analytical method and global finite differences method. Finally, by integrating the algorithm mentioned based on RKPM with parameterized descriptive method of boundary shape, two examples for structural dynamic shape optimization are performed.

Keywords Meshless method · Reproducing kernel particle method · Dynamic sensitivity analysis · Dynamic optimization design · Shape optimization

J. P. Zhang · S. G. Gong (✉) · A. H. Qiu · R. K. Chen
School of Mechanical Engineering, Xiangtan University, Xiangtan 411105, People's Republic of China
e-mail: gongsg@xtu.edu.cn

S. G. Gong · Y. Q. Huang
Hunan Key Laboratory for Computation and Simulation in Science and Engineering, Xiangtan University, Xiangtan 411105, People's Republic of China

1 Introduction

The designers have to control the natural frequency or dynamic response and so on to realize the dynamics design target (such as avoiding harmful resonance vibration and excessive vibration assurance of dynamic stability) of engineering structure (Rong et al. 2002). Structural dynamic shape optimization aims for improving the structural dynamic property and saving in weight by adjusting inner and outer boundary of structure (Gu et al. 2005). There are numerous difficulties such as mesh distortion, a large number of remeshes that effect both computational accuracy and efficiency during the dynamic shape optimization process using finite element method (FEM). The emerging meshless method based on node interpolation can resolve the above-mentioned problems radically. Reproducing kernel particle method (RKPM) is a meshless method that generates shape functions using reproducing kernel approximation, and it is widely applied in structural dynamics (Liu et al. 1995; Zhou et al. 2005a, b).

The gradient-based optimization algorithm depends on the sensitivity analysis to a great extent. Methods of sensitivity analysis sort discrete approach and variational approach according to calculated strategy and are solved mostly by using FEM, semi-analytical method (SAM), and global finite differences method (GFDM; Keulen et al. 2005).

Study on design-sensitivity analysis and shape optimization based on meshless method has attracted some scholars' attention, but that achievement is mainly confined to static problems (Zhang et al. 2005; Grindeanu et al. 1999; Kim et al. 2000; Bobaru and Mukherjee 2001; Kim et al. 2003; Zhou et al. 2005a, b; Gong et al. 2006a, b). In structural dynamic optimization problems, functional feature and sensitivity analysis are far more complicated than those in structural static optimization, for the reason that both

objective and constraint function are high-order nonlinear, implicit, and compound function of design variable (Liao et al. 2003); moreover, conventional methods are usually based on FEM or boundary element method (BEM). Yoo et al. (2006) performed shape optimization of rotating cantilever beams with frequency constraint. Bogomolni et al. (2006) proposed an efficient method of dynamic design sensitivity by integrating combined approximation and finite differences. Falco et al. (2004a, b) accomplished dynamic sensitivity analysis and shape optimization of square plate and cylindrical shell. Kim and Choi (2001) used RKPM and continuum derivatives to study design sensitivity analysis of structural nonlinear transient dynamics for the finite deformation elasto-plastic materials under impact with a rigid surface, and then shape optimization of vehicle bumper was achieved. The continuum-based sensitivity equation was obtained by differentiating the weak form of the equations of motion for a structural dynamic problem with respect to the design variables, but the sensitivity of natural frequency is not developed.

In this paper, we develop a numerical method of structural dynamic shape optimization in the RKPM context. The penalty method is employed into imposing the essential boundary condition, and the discrete natural frequency sensitivity equation and dynamic response sensitivity equation based on RKPM are proposed by using direct differentiation method (DDM) and discrete derivatives (Bogomolni et al. 2006) on the basis of structural dynamic analysis. Results obtained by DDM are compared with SAM and GFDM, and those results match well. Finally, the above algorithm of optimization based on RKPM and parameterized descriptive methods of boundary shape are utilized, and dynamic shape optimization of two engineering models is performed mostly in the perspective of dynamic property.

This paper is organized as follows: In section 2, we briefly describe the reproducing kernel approximation and the discrete dynamic equation based on RKPM with a penalty method for imposing the essential boundary conditions. In section 3, we formulate the discrete natural frequency sensitivity equation and discrete dynamic response sensitivity equation, in the context of RKPM, and the design derivatives of the RKPM shape function and its spatial derivatives, using DDM. In section 4, we firstly use two numerical examples, i.e., a cantilever beam with impact load and an arc, for testing the accuracy of free frequencies and displacement response along with their sensitivity analysis. Comparisons with results using the FEM and GFDM are made. Structural dynamic shape optimization of an arc and a fillet are then performed with RKPM using derived sensitivities and parameterized descriptive methods of boundary shape. Finally, the paper ends with some conclusions.

2 Basic theory and dynamic analysis

2.1 Reproducing kernel approximation

Reproducing kernel approximation (Liu et al. 1995) regularizes the displacement $\mathbf{u}(\mathbf{x})$, using the kernel function and the correction function. For given domain $\mathbf{\Omega}\in R^2$, suppose that the domain $\mathbf{\Omega}$ is discretized by a set of distinct particles $[\mathbf{x}_1,\mathbf{x}_2,...,\mathbf{x}_{IP}]$, where $\mathbf{x}_I$ is the location of particle I, IP is the total number of particles, and then in the case of two-dimensional problem, the reproducing kernel approximation of displacement $\mathbf{u}(\mathbf{x})$ is

$$\mathbf{u}^{\mathrm{h}}(\mathbf{x}) = \sum_{I=1}^{IP} C(\mathbf{x};\mathbf{x}_I-\mathbf{x})\omega(\mathbf{x}_I-\mathbf{x})\mathbf{u}_I\Delta x_I = \sum_{I=1}^{IP}\phi_I(\mathbf{x})\mathbf{u}_I \quad (1)$$

Where $\mathbf{u}^{\mathrm{h}}(\mathbf{x})$ is the reproduced displacement of $\mathbf{u}(\mathbf{x})$, a 2×1 vector; $C(\mathbf{x};\mathbf{x}_I-\mathbf{x})$ is the correction function, $\omega(\mathbf{x}_I-\mathbf{x})$ is the kernel function, and $\mathbf{u}_I$ is the generalized displacement of particle $\mathbf{x}_I$, a 2×1 vector. $\phi_I(\mathbf{x})$ is the RKPM shape function for particle $\mathbf{x}_I$, and it can be written in the form of matrix as follows

$$\mathbf{\Phi}(\mathbf{x}) = [\phi_1(\mathbf{x}),\phi_2(\mathbf{x}),\cdots,\phi_{IP}(\mathbf{x})] = \mathbf{p}^{\mathrm{T}}(0)\mathbf{A}^{-1}(\mathbf{x})\mathbf{H}(\mathbf{x}) \quad (2)$$

Where

$$\mathbf{A}(\mathbf{x}) = \sum_{I=1}^{IP}\omega(\mathbf{x}_I-\mathbf{x})\mathbf{p}(\mathbf{x}_I-\mathbf{x})\mathbf{p}^{\mathrm{T}}(\mathbf{x}_I-\mathbf{x})\Delta x_I \quad (3)$$

$$\mathbf{H}(\mathbf{x}) = \begin{bmatrix}\mathbf{p}(\mathbf{x}_1-\mathbf{x})\omega(\mathbf{x}_1-\mathbf{x})\Delta x_1, \mathbf{p}(\mathbf{x}_2-\mathbf{x})\omega(\mathbf{x}_2-\mathbf{x})\Delta x_2,\cdots,\\ \mathbf{p}(\mathbf{x}_I-\mathbf{x})\omega(\mathbf{x}_I-\mathbf{x})\Delta x_I\end{bmatrix} \quad (4)$$

$$\mathbf{p}(\mathbf{x}_I-\mathbf{x}) = [1, x_I-x, y_I-y]^{\mathrm{T}} \quad (5)$$

$\mathbf{\Phi}(\mathbf{x})$ is a $1\times IP$ vector, $\mathbf{A}(\mathbf{x})$ is a 3×3 matrix, and $\mathbf{H}(\mathbf{x})$ is a $3\times IP$ matrix. $\mathbf{p}(\mathbf{x}_I-\mathbf{x})$ is a linear basis in two dimensions (2D), and Δx_I is a measure of the weight associated with particle $\mathbf{x}_I$. As a result that the effect of Δx_I will be counterbalanced in practice, for simplicity, $\Delta x_I=1$ (Kim et al. 2003).

The kernel function plays an important role in the reproducing kernel approximation. In this paper, the following cubic spline function (Kim et al. 2003) is utilized for the kernel function that has a second-order continuous property.

$$\omega(r) = \frac{1}{6}\begin{cases}(3r^3-6r^2+4), & 0\le r\le 1\\ -(r-2)^3, & 1\le r\le 2\\ 0, & \text{otherwise}\end{cases} \quad (6)$$

In 2D,

$$\omega(\mathbf{x}_I-\mathbf{x}) = \frac{1}{d_{mx}}\omega(r_x)\frac{1}{d_{my}}\omega(r_y) \quad (7)$$

Where $r_x = \|(x_I - x)\|/d_{mx}$, $r_y = \|(y_I - y)\|/d_{my}$, d_{mx} and d_{my} are the x-dimensional and y-dimensional radii of influential domain corresponding to the particle $\mathbf{x}_I$, respectively. In this paper, we choose d_{mx}=scale×c_{Ix} and d_{my}= scale×c_{Iy}, where scale is a scaling parameter, and an acceptable result can be obtained when it is chosen in the range of 1.0~3.0; c_{Ix} and c_{Iy} are the shortest distances between the particle $\mathbf{x}_I$ and neighbor particles in the x-direction and y-direction separately.

The radius of influential domain should be large enough to provide a sufficient number of particles in the support domain and to ensure invertibility of the matrix $\mathbf{A}(\mathbf{x})$ in (3); on the other hand, the radius should not be too large, otherwise, the local character of the reproducing kernel approximation which constitutes an essential property of the RKPM will be lost, and this also can lead to ill-conditioned system matrices. During optimization, the radius of influential domain is not fixed and changes along with the density of the scattered particles. The radius is larger when the particles distribute sparsely, while the radius is smaller when the particles distribute densely.

To calculate the spatial derivatives of the shape function $\mathbf{\Phi}(\mathbf{x})$, (2) can be differentiated directly with respect to coordinate $\mathbf{X}$ as follows

$$\begin{aligned}\mathbf{\Phi}_{,\mathbf{X}}(\mathbf{x}) &= \left[\phi_{1,\mathbf{X}}(\mathbf{x}), \phi_{2,\mathbf{X}}(\mathbf{x}), \cdots, \phi_{IP,\mathbf{X}}(\mathbf{x})\right] \\ &= \mathbf{p}^{\mathrm{T}}(0)\left(\mathbf{A}^{-1}_{,\mathbf{X}}(\mathbf{x})\mathbf{H}(\mathbf{x}) + \mathbf{A}^{-1}(\mathbf{x})\mathbf{H}_{,\mathbf{X}}(\mathbf{x})\right)\end{aligned} \tag{8}$$

Where

$$\mathbf{A}^{-1}_{,\mathbf{X}}(\mathbf{x}) = -\mathbf{A}^{-1}\mathbf{A}_{,\mathbf{X}}\mathbf{A}^{-1} \tag{9}$$

$$\mathbf{A}_{,\mathbf{X}}(\mathbf{x}) = \sum_{I=1}^{IP}\begin{pmatrix}\omega_{,\mathbf{X}}(\mathbf{x}_I - \mathbf{x})\mathbf{p}(\mathbf{x}_I - \mathbf{x})\mathbf{p}^{\mathrm{T}}(\mathbf{x}_I - \mathbf{x}) \\ +\omega(\mathbf{x}_I - \mathbf{x})\mathbf{p}_{,\mathbf{X}}(\mathbf{x}_I - \mathbf{x})\mathbf{p}^{\mathrm{T}}(\mathbf{x}_I - \mathbf{x}) \\ +\omega(\mathbf{x}_I - \mathbf{x})\mathbf{p}(\mathbf{x}_I - \mathbf{x})\mathbf{p}^{\mathrm{T}}_{,\mathbf{X}}(\mathbf{x}_I - \mathbf{x})\end{pmatrix} \tag{10}$$

$$\mathbf{H}_{,\mathbf{X}}(\mathbf{x}) = \begin{bmatrix}\mathbf{p}_{,\mathbf{X}}(\mathbf{x}_1 - \mathbf{x})\omega(\mathbf{x}_1 - \mathbf{x}) + \mathbf{p}(\mathbf{x}_1 - \mathbf{x})\omega_{,\mathbf{X}}(\mathbf{x}_1 - \mathbf{x}), \\ \mathbf{p}_{,\mathbf{X}}(\mathbf{x}_2 - \mathbf{x})\omega(\mathbf{x}_2 - \mathbf{x}) + \mathbf{p}(\mathbf{x}_2 - \mathbf{x})\omega_{,\mathbf{X}}(\mathbf{x}_2 - \mathbf{x}), \ldots, \\ \mathbf{p}_{,\mathbf{X}}(\mathbf{x}_I - \mathbf{x})\omega(\mathbf{x}_I - \mathbf{x}) + \mathbf{p}(\mathbf{x}_I - \mathbf{x})\omega_{,\mathbf{X}}(\mathbf{x}_I - \mathbf{x})\end{bmatrix} \tag{11}$$

Where $\mathbf{\Phi}_{,\mathbf{x}}(\mathbf{x})$ is a $1\times IP$ vector, $\mathbf{A}_{,\mathbf{x}}(\mathbf{x})$ is a 3×3 matrix, $\mathbf{H}_{,\mathbf{x}}(\mathbf{x})$ is a $3\times IP$ matrix, and the subscript "$_{,\mathbf{x}}$" denotes the first-order partial derivative $\partial/\partial\mathbf{X}$, namely, $\partial/\partial x$ or $\partial/\partial y$ in 2D.

2.2 The discrete dynamic equations

As a result that the shape function of RKPM usually does not verify the Kronecker delta property, direct imposition of essential boundary conditions for RKPM is difficult. So far, many specific methods for the implementation of essential boundary conditions for RKPM have been developed, for example, the Lagrange multiplier method, the penalty method, the modified variational principle, and so on. The Lagrange multiplier method introduces a new unknown function, the Lagrange multiplier, and increases the number of unknowns. The system stiffness matrix resulting from the Lagrange multiplier method will no longer be positive-definite.

The penalty method (Bobaru and Mukherjee 2001) does not increase the number of unknowns and yields a symmetric and positive-definite linear system, which is a significant advantage in practical applications. An important consideration for using the penalty method is the choice of an appropriate penalty factor α. The penalty factor α cannot be taken "very large", otherwise, the system stiffness matrix may become ill-conditioned. From our tests, the results with good accuracy can be obtained in dynamic problem when the penalty factor α is chosen anywhere between 3.0×10^3E and 3.0×10^5E, where E is the Young's modulus of the material under consideration.

In this paper, the penalty method is used in implementation essential boundary conditions for the case of plane problem, and then structural free vibration equation and dynamical equation based on RKPM are formulated as

$$\left(\mathbf{K} + \mathbf{K}_\alpha - \omega^2\mathbf{M}\right)\mathbf{Q} = 0 \tag{12}$$

$$\mathbf{M}\ddot{\mathbf{u}}(t) + \mathbf{C}\dot{\mathbf{u}}(t) + (\mathrm{K} + \mathrm{K}_\alpha)\mathbf{u}(t) = \mathbf{F}(t) + \mathbf{F}_\alpha(t) \tag{13}$$

Where the initial displacement and velocity are zero, namely, $u(t)|_{t=0} = \dot{u}(t)\Big|_{t=0} = 0$.The global $(2\times IP)\times(2\times IP)$ matrices $\mathbf{K}$, $\mathbf{K}_\alpha$, $\mathbf{M}$, and $\mathbf{C}$ are gathered from the following 2×2 submatrices $\mathbf{K}_{IJ}$, $K_{\alpha IJ}$, $\mathbf{M}_{IJ}$, and $\mathbf{C}_{IJ}$ (I,J=1,2, ...,IP)

$$\mathbf{K}_{IJ} = \int_\Omega \mathbf{B}_I^{\mathrm{T}}\mathbf{D}\mathbf{B}_J \mathrm{d}\Omega \tag{14}$$

$$\mathbf{K}_{\alpha IJ} = \alpha\int_{\Gamma_u} \Phi_I^{\mathrm{T}}\Phi_J \mathrm{d}\Gamma \tag{15}$$

$$\mathbf{M}_{IJ} = \int_\Omega \rho\Phi_I^{\mathrm{T}}\Phi_J \mathrm{d}\Omega \tag{16}$$

$$\mathbf{C}_{IJ} = \beta_0\mathbf{M}_{IJ} + \beta_1(\mathbf{K}_{IJ} + \mathbf{K}_{\alpha IJ}) \tag{17}$$

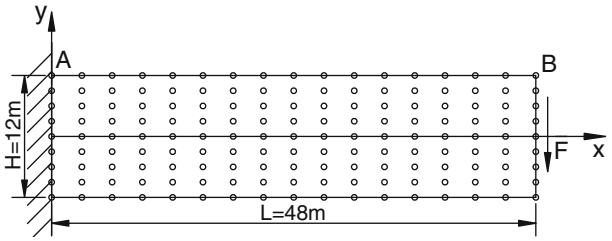

Fig. 1 Node distribution of the cantilever beam

in which

$$\mathbf{B}_I = \begin{bmatrix} \phi_{I,x} & 0 \\ 0 & \phi_{I,y} \\ \phi_{I,y} & \phi_{I,x} \end{bmatrix} \tag{18}$$

$$\mathbf{\Phi}_I = \begin{bmatrix} \phi_I & 0 \\ 0 & \phi_I \end{bmatrix} \tag{19}$$

$\mathbf{B}_I$ is the 3×2 matrix, $\mathbf{\Phi}_I$ is the 2×2 diagonal matrix.

Similarly, the $(2\times IP)\times 1$ vectors $\mathbf{F}(t)$ and $F_\alpha(t)$) are constructed from the following 2×1 subvectors $\mathbf{F}(t)_I$ and $F_\alpha(t)_I$ (I=1,2, ...,IP)

$$\mathbf{F}(t)_I = \int_\Omega \Phi_I^{\mathrm{T}} Z \mathrm{d}\Omega + \int_{\Gamma_t} \Phi_I^{\mathrm{T}} \mathbf{f}(t) \mathrm{d}\Gamma + \sum_{k=1}^{n_k} \Phi_I^{\mathrm{T}}(\mathbf{x}_k) \mathbf{T}_k(\mathbf{x}_k, t) \tag{20}$$

$$\mathbf{F}_\alpha(t)_I = \alpha \int_{\Gamma_u} \overline{\mathrm{u}}\, \Phi_I^{\mathrm{T}} \mathrm{d}\Gamma \tag{21}$$

where, ω—circular frequency; **Q**—eigenvector matrices; **M**, **C**, **K**, and K_α—mass matrices, damping matrices, stiffness matrices, and corresponding penalty item; $\ddot{\mathbf{u}}(t)$, $\mathbf{u}(t)$, and $\mathbf{u}(t)$—acceleration, velocity, and displacement column vectors; $\mathbf{F}(t)$ and $\mathbf{F}_\alpha(t)$—load column vector and corresponding penalty item; **D**—elasticity matrix for the plane stress case; β_0 and β_1—proportional damping constant; **Z**, $\mathbf{f}(t)$, $\mathbf{T}_k(\mathbf{x}_k, t)$, n_k, and x_k—body force, surface force, concentrated force, and the number and the acting position of concentrated force; $\overline{\mathbf{u}}$—given boundary displacement.

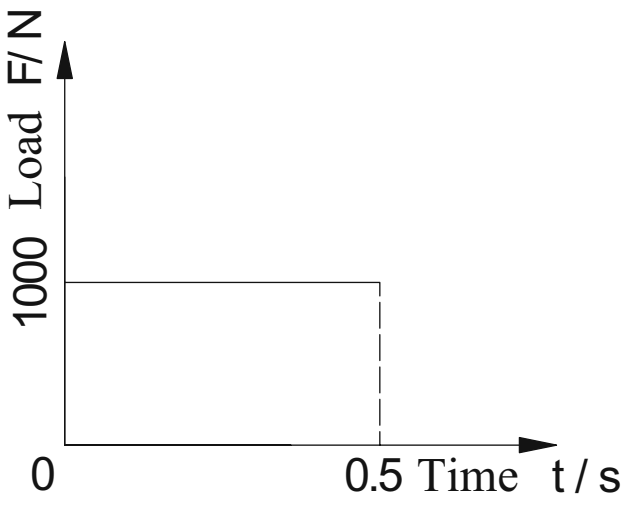

Fig. 2 Impact load time history record

Before (12) and (13) are solved, we need to evaluate the integrals (14), (15), (16), (20), and (21). To evaluate these integrals, we used a cell structure which is independent of particles and has the discretization particles at its corner. The cells are arranged in a regular pattern and used to perform integration like the FEM elements.

Equations (12) and (13) can be solved by using subspace iteration method and *Wilson-θ* method, respectively. Their solution procedure is similar to FEM, and the detailed process refers to Liao et al. (2003).

We should notice that the computational cost of RKPM is usually higher than FEM. The construction of RKPM shape functions is more delicate and time-consuming than evaluation of FEM shape functions, as a result that lots of calculation of inverting matrices is needed. In addition, the bandwidths of all matrices from RKPM are generally larger than that from the traditional FEM, as the radius of influential domain in RKPM cannot be too small. The bandwidths of these matrices are also affected by the integration cell structure and the number of Gauss points in each cell.

3 Dynamic optimal models and the design velocity field

Structural dynamic optimization generally aims at minimizing the weight of the structure which is under natural frequency or displacement response constraints (Grandhi 1993), and the optimization design model is

$$\min W(\mathbf{b}) \tag{22}$$
$$\text{s.t.} \begin{cases} g_i(\mathbf{b}) \geq 0 & (i = 1, 2, \cdots, m) \\ b_j^L \leq b_j \leq b_j^U & (j = 1, 2, \cdots, n) \end{cases}$$

Where $\mathbf{b}=[b_1,b_2,...,b_n]$ is the vector of design variables, $W(\mathbf{b})$ is the objective function, $g_i(\mathbf{b})$ is the ith performance constraint condition, b_j, b_j^L, and b_j^U are the jth design

Table 1 First five natural frequencies of the beam (unit: hertz)

Modal	1	2	3	4	5
RKPM	4.396	22.568	28.669	52.390	85.604
FEM	4.422	22.658	28.629	52.616	85.776

Table 2 Sensitivities of the first five natural frequencies of the beam (unit: hertz per meter)

Modal	1	2	3	4	5
DDM	−0.339708	−1.081912	−0.004308	−1.683438	−1.739785
SAM	−0.315693	−1.053537	−0.004586	−1.699361	−1.726695
GFDM	−0.316461	−1.065523	−0.004471	−1.724155	−1.748333

variable and its upper and lower bound, and m and n are the number of performance constraint condition and design variable, respectively.

The boundary shape is usually described with the parametric curve or curve surface based on structural geometrical feature. Suppose that the initial structural domain Ω is changed into the perturbed domain Ω_τ in which the parameter t controls the shape perturbation amount. By defining the design velocity field to be $\mathbf{V}(\mathbf{x})$ (Bobaru and Mukherjee 2001; Gong et al. 2006a, b), the material point after perturbation can be denoted as $\mathbf{x}_\tau = \mathbf{x} + t\mathbf{V}(\mathbf{x})$.

What is more, we should notice that structural dynamic optimization design is a typical inverse problem of dynamics (Rong et al. 2002). In this paper, the optimization is performed on the premise of the existence and uniqueness of the optimum solution.

4 Structural dynamic sensitivity analysis

Structural dynamic sensitivity analysis mainly includes the sensitivity analysis of structural natural frequency and dynamic response. In the course of sensitivity analysis, the most distinctive difference between FEM and RKPM is that the design derivative of the FEM shape function which depends on the reference geometry is zero, and that of the RKPM shape function which depends on the global coordinates of material points (Kim et al. 2003) is nonzero. In other words, in FEM, the design derivative of the spatial derivatives of the shape function is calculated only, and without considering the design derivative of the shape function, while in RKPM, both of them must be taken into account.

4.1 Natural frequency sensitivity analysis

Using the DDM, the derivative of (12) with respect to the jth design variable $b_j (j=1,2, ...,b_n)$, namely, the structural natural frequency sensitivity equation, is given by

$$\begin{aligned}&\left(\mathbf{K}_{,b_j} + \mathbf{K}_{\alpha,b_j} - 2\omega\omega_{,b_j}\mathbf{M} - \omega^2\mathbf{M}_{,b_j}\right)\mathbf{Q} \\ &+ \left(\mathbf{K} + \mathbf{K}_\alpha - \omega^2\mathbf{M}\right)\mathbf{Q}_{,b_j} \\ &= 0\end{aligned} \tag{23}$$

By left-multiplying (23) by $\mathbf{Q}^{\mathrm{T}}$ and integrating (12) and the normalization of mass matrices: $\mathbf{Q}^{\mathrm{T}}\mathbf{M}\mathbf{Q}=1$, the frequency sensitivity $\omega_{,b_j}$ can be obtained by

$$\omega_{,b_j} = \mathbf{Q}^{\mathrm{T}}\left(\mathbf{K}_{,b_j} + \mathbf{K}_{\alpha,b_j} - \omega^2\mathbf{M}_{,b_j}\right)\mathbf{Q}/2\omega \tag{24}$$

Where the global $(2\times IP)\times(2\times IP)$ matrices $\mathbf{K}_{,b_j}$, $\mathbf{K}_{\alpha,b_j}$, and $\mathbf{M}_{,b_j}$ are constructed from the following 2×2 submatrices $\mathbf{K}_{IJ,b_j}$, $\mathbf{K}_{\alpha IJ,b_j}$, and $\mathbf{M}_{IJ,b_j}$ (I, J=1,2, ...,IP)

$$\mathbf{K}_{IJ,b_j} = \int_\Omega \left(\mathbf{B}_{I,b_j}^{\mathrm{T}}\mathbf{D}\mathbf{B}_J + \mathbf{B}_I^{\mathrm{T}}\mathbf{D}\mathbf{B}_{J,b_j} + \mathbf{B}_I^{\mathrm{T}}\mathbf{D}\mathbf{B}_J \mathrm{div}\mathbf{V}\right)\mathrm{d}\Omega \tag{25}$$

$$\mathbf{K}_{\alpha IJ,b_j} = \alpha\int_{\Gamma_u}\left[\Phi_{I,b_j}^{\mathrm{T}}\Phi_J + \Phi_I^{\mathrm{T}}\Phi_{J,b_j} + \Phi_I^{\mathrm{T}}\Phi_J(\mathbf{V}\cdot\mathbf{n})H\right]\mathrm{d}\Gamma \tag{26}$$

$$\mathbf{M}_{IJ,b_j} = \int_\Omega \rho\left(\Phi_{I,b_j}^{\mathrm{T}}\Phi_J + \Phi_I^{\mathrm{T}}\Phi_{J,b_j} + \Phi_I^{\mathrm{T}}\Phi_J \mathrm{div}\mathbf{V}\right)\mathrm{d}\Omega \tag{27}$$

in which

$$\mathbf{B}_{I,b_j} = \begin{bmatrix} \phi_{I,xb_j} & 0 \\ 0 & \phi_{I,yb_j} \\ \phi_{I,yb_j} & \phi_{I,xb_j} \end{bmatrix} \tag{28}$$

$$\Phi_{I,b_j} = \begin{bmatrix} \phi_{I,b_j} & 0 \\ 0 & \phi_{I,b_j} \end{bmatrix} \tag{29}$$

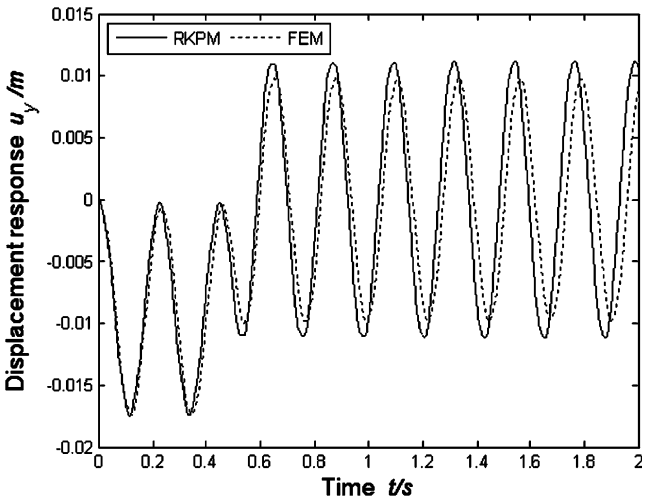

Fig. 3 Displacement response u_y at point B

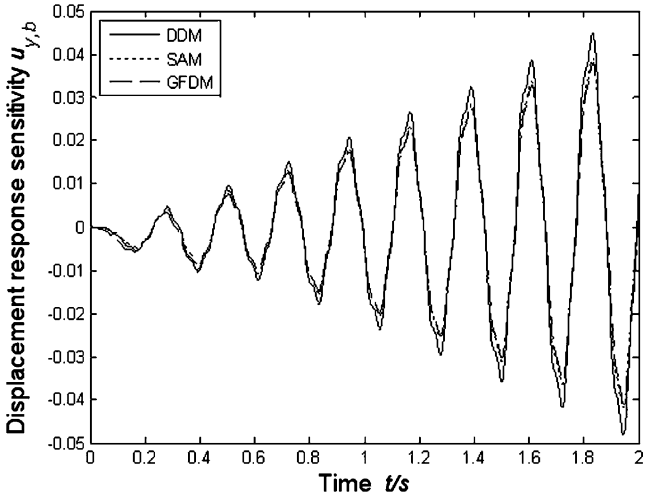

Fig. 4 Displacement response sensitivity u_{yb} at point B

Where $\mathbf{B}_{I,b_j}$ is the 3×2 matrix, Φ_{I,b_j} is the 2×2 diagonal matrix, H=div$\mathbf{n}$ is the curvature of Γ in 2D, $\mathbf{n}$ is the unit normal to the boundary Γ, and the subscript "b_j" denotes the first-order partial derivative $\partial/\partial b_j$.

4.2 Dynamic response sensitivity analysis

Using the DDM, differentiate (13) with respect to the jth design variable b_j(j=1,2, ...,n) and rearrange, and then the structural dynamic response sensitivity equation is given by

$$\begin{aligned}&\mathbf{M}\ddot{\mathbf{u}}(t)_{,b_j}+\mathbf{C}\dot{\mathbf{u}}(t)_{,b_j}+(\mathbf{K}+\mathbf{K}_\alpha)\mathbf{u}(t)_{,b_j}\\&=\mathbf{F}(t)_{,b_j}+\mathbf{F}_\alpha(t)_{,b_j}-\mathbf{M}_{,b_j}\ddot{\mathbf{u}}(t)-\mathbf{C}_{,b_j}\dot{\mathbf{u}}(t)\\&\quad-\left(\mathbf{K}_{,b_j}+\mathbf{K}_{\alpha,b_j}\right)\mathbf{u}(t)\end{aligned}\tag{30}$$

Considering the right-hand sides of (30) as the generalized load column vector $\mathbf{F}^*(t)+\mathbf{F}^*_\alpha(t)$, where $\mathbf{F}^*(t)+\mathbf{F}^*_\alpha(t)$ is defined as

$$\begin{aligned}\mathbf{F}^*(t)+\mathbf{F}^*_\alpha(t)&=\mathbf{F}(t)_{,b_j}+\mathbf{F}_\alpha(t)_{,b_j}-\mathbf{M}_{,b_j}\ddot{\mathbf{u}}(t)\\&\quad-\mathbf{C}_{,b_j}\dot{\mathbf{u}}(t)-\left(\mathbf{K}_{,b_j}+\mathbf{K}_{\alpha,b_j}\right)\mathbf{u}(t)\end{aligned}\tag{31}$$

then (30) is transformed to

$$\begin{aligned}&\mathbf{M}\ddot{\mathbf{u}}(t)_{,b_j}+\mathbf{C}\dot{\mathbf{u}}(t)_{,b_j}+(\mathbf{K}+\mathbf{K}_\alpha)\mathbf{u}(t)_{,b_j}\\&=\mathbf{F}^*(t)+\mathbf{F}^*_\alpha(t)\end{aligned}\tag{32}$$

It is obvious that (32) and (13) are very similar in terms of form and have identical coefficient matrices. According to the above advantages, (32) can be solved by using the same solution method as (13); the only need is to modify a little part of original computation program for structural dynamic analysis based on RKPM, so that the structural displacement response sensitivity $\mathbf{u}(t)_{,b_j}$ can be obtained easily, and so are the sensitivities of the velocity and acceleration $\dot{\mathbf{u}}(t)_{,b_j}$ and $\mathbf{u}(t)_{,b_j}$. Where the initial sensitivities of the displacement and velocity are zero, namely, $\mathbf{u}(t)_{,b_j}\big|_{t=0}=\dot{\mathbf{u}}(t)_{,b_j}\big|_{t=0}=0$. The global $(2\times IP)\times(2\times IP)$ matrices $\mathbf{C}_{,b_j}$ is gathered from the following 2×2 submatrices $\mathbf{C}_{IJ,b_j}$ $(I,J=1,2,...,IP)$

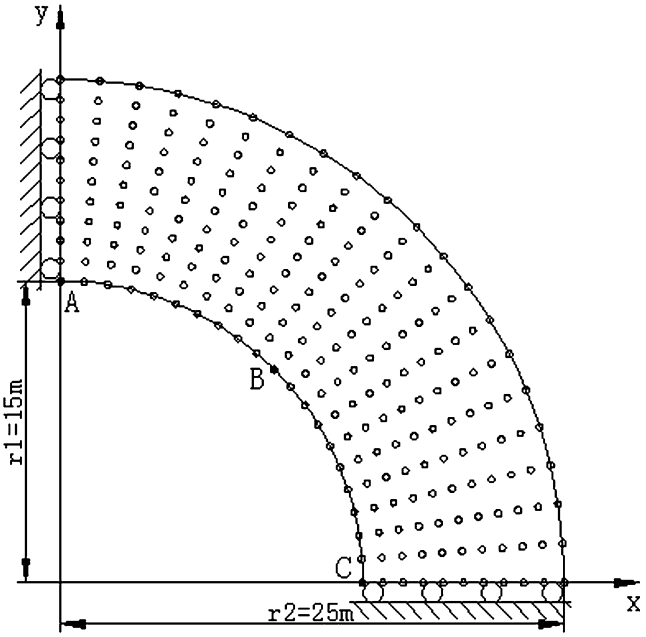

Fig. 5 Node distribution of the arc

$$\mathbf{C}_{IJ,b_j}=\beta_0\mathbf{M}_{IJ,b_j}+\beta_1\left(\mathbf{K}_{IJ,b_j}+\mathbf{K}_{\alpha IJ,b_j}\right)\tag{33}$$

Suppose that the impact loads are independent of the jth design variable b_j, and then the derivatives of the load column vector and corresponding penalty item with respect to the jth design variable b_j, the $(2\times IP)\times 1$ vectors $\mathbf{F}(t)_{,b_j}$ and $\mathbf{F}_\alpha(t)_{,b_j}$ consist of the following 2×1 subvectors $\mathbf{F}(t)_{I,b_j}$ and $\mathbf{F}_\alpha(t)_{I,b_j}(I=1,2,\cdots,IP)$

$$\begin{aligned}\mathbf{F}(t)_{I,b_j}&=\int_\Omega\left(\Phi^T_{I,b_j}+\Phi^T_I\mathrm{div}\mathbf{V}\right)\mathbf{Z}\mathrm{d}\Omega\\&\quad+\int_{\Gamma_t}\left[\Phi^{\mathrm{T}}_{I,b_j}+\Phi^T_I(\mathbf{V}\cdot\mathbf{n})H\right]\mathbf{f}(t)\mathrm{d}\Gamma\\&\quad+\sum_{k=1}^{n_k}\Phi^{\mathrm{T}}_{I,b_j}(\mathbf{x}_k)\mathrm{T}_k(\mathbf{x}_k,t)\end{aligned}\tag{34}$$

$$\mathbf{F}_\alpha(t)_{I,b_j}=\alpha\int_{\Gamma_u}\bar{\mathbf{u}}\left[\Phi^{\mathrm{T}}_{I,b_j}+\Phi^{\mathrm{T}}_I(\mathbf{V}\cdot\mathbf{n})\mathrm{H}\right]\mathrm{d}\Gamma\tag{35}$$

Table 3 First five natural frequencies of the arc (unit: hertz)

Modal	1	2	3	4	5
RKPM	14.105	41.877	59.904	84.923	112.450
FEM	14.434	41.953	60.843	85.232	113.270

Table 4 Sensitivities of the first five natural frequencies of the arc (unit: hertz per meter)

Modal	1	2	3	4	5
DDM	−1.762361	−1.281255	−5.278611	−0.386944	−7.663057
SAM	−1.775608	−1.227960	−5.425695	−0.396699	−7.471683
GFDM	−1.845927	−1.283732	−5.503777	−0.410477	−7.338454

4.3 Derivatives of shape function

To determine the sensitivity of structural natural frequency and dynamic response, the derivatives of the shape function $\Phi(\mathbf{x})$ and its spatial derivatives $\Phi_{,\mathbf{x}}(\mathbf{x})$ with respect to the jth design variable b_j should be evaluated.

Differentiating (2) with respect to the jth design variable b_j directly and the design derivative of the RKPM shape function, $\Phi_{,b_j}(\mathbf{x})$ is given by

$$\begin{aligned}\Phi_{,b_j}(\mathbf{x}) &= \left[\phi_{1,b_j}(\mathbf{x}), \phi_{2,b_j}(\mathbf{x}), \cdots, \phi_{IP,b_j}(\mathbf{x})\right] \\ &= \mathbf{p}^{\mathrm{T}}(0)\left(\mathbf{A}^{-1}_{,b_j}(\mathbf{x})\mathbf{H}(\mathbf{x}) + \mathbf{A}^{-1}(\mathbf{x})\mathbf{H}_{,b_j}(\mathbf{x})\right)\end{aligned} \tag{36}$$

Where

$$\mathbf{A}^{-1}_{,b_j}(\mathbf{x}) = -\mathbf{A}^{-1}\mathbf{A}_{,b_j}\mathbf{A}^{-1} \tag{37}$$

$$\begin{aligned}\mathbf{A}_{,b_j}(\mathbf{x}) = \sum_{I=1}^{IP} &(\omega_{,b_j}(\mathbf{x}_I - \mathbf{x})\mathbf{p}(\mathbf{x}_I - \mathbf{x})\mathbf{p}^{\mathrm{T}}(\mathbf{x}_I - \mathbf{x}) \\ &+ \omega(\mathbf{x}_I - \mathbf{x})\mathbf{p}_{,b_j}(\mathbf{x}_I - \mathbf{x})\mathbf{p}^{T}(\mathbf{x}_I - \mathbf{x}) \\ &+ \omega(\mathbf{x}_I - \mathbf{x})\mathbf{p}(\mathbf{x}_I - \mathbf{x})\mathbf{p}^{\mathrm{T}}_{,b_j}(\mathbf{x}_I - \mathbf{x}))\end{aligned} \tag{38}$$

$$\begin{aligned}\mathbf{H}_{,b_j}(\mathbf{x}) = [&\mathbf{p}_{,b_j}(\mathbf{x}_1 - \mathbf{x})\omega(\mathbf{x}_1 - \mathbf{x}) + \mathbf{p}(\mathbf{x}_1 - \mathbf{x})\omega_{,b_j}(\mathbf{x}_1 - \mathbf{x}), \\ &\mathbf{p}_{,b_j}(\mathbf{x}_2 - \mathbf{x})\omega(\mathbf{x}_2 - \mathbf{x}) + \mathbf{p}(\mathbf{x}_2 - \mathbf{x})\omega_{,b_j}(\mathbf{x}_2 - \mathbf{x}), \\ &\cdots, \mathbf{p}_{,b_j}(\mathbf{x}_1 - \mathbf{x})\omega(\mathbf{x}_1 - \mathbf{x}) + \mathbf{p}(\mathbf{x}_1 - \mathbf{x})\omega_{,b_j}(\mathbf{x}_1 - \mathbf{x})]\end{aligned} \tag{39}$$

$$\mathbf{p}_{,b_j}(\mathbf{x}_I - \mathbf{x}) = \left[1, V^I_x - V_x, V^I_y - V_y\right]^{\mathrm{T}} \tag{40}$$

$$\omega_{,b_j}(r) = \frac{1}{2}\begin{cases}(3r^2 - 4r), & 0 \le r \le 1 \\ -(r-2)^2, & 1 \le r \le 2 \\ 0, & \text{otherwise}\end{cases} \tag{41}$$

In 2D,

$$\begin{aligned}&\omega_{,b_j}(\mathbf{x}_I - \mathbf{x}) \\ &= \frac{(V^I_x - V_x)(\mathrm{sign}(V^I_x - V_x))}{d^2_{mx}}\omega_{,b_j}(r_x)\frac{\left(V^I_y - V_y\right)\left(\mathrm{sign}\left(V^I_y - V_y\right)\right)}{d^2_{my}}\omega_{,b_j}(r_y)\end{aligned} \tag{42}$$

Where V^I_x, V^I_y, V_x, and V_y are the components of the design velocity in the x and y directions at $\mathbf{x}_I$ and at $\mathbf{x}$, respectively. When the design velocity is given, (36) can be explicitly evaluated before sensitivity analysis. It should be noted that the design velocity is generally unknown in practical optimal problem, and under such situation, the design velocity can be calculated by using finite differences method (FDM) (Francavilla et al. 1975).

Similarly, differentiating (8) with respect to the jth design variable b_j directly, the design derivative of the spatial derivatives of the shape function, $\Phi_{,Xb_j}(\mathbf{x})$ is obtained

$$\begin{aligned}\Phi_{,\mathrm{X}b_j}(\mathbf{x}) &= \left[\phi_{1,\mathrm{X}b_j}(\mathbf{x}), \phi_{2,\mathrm{X}b_j}(\mathbf{x}), \cdots, \phi_{IP,\mathrm{X}b_j}(\mathbf{x})\right] \\ &= \mathrm{p}^{\mathrm{T}}(0)\begin{pmatrix}\mathrm{A}^{-1}_{,\mathrm{X}b_j}(\mathrm{x})\mathrm{H}(\mathrm{x}) + \mathrm{A}^{-1}_{,\mathrm{X}}(\mathrm{x})\mathrm{H}_{,b_j}(\mathrm{x}) + \\ \mathbf{A}^{-1}_{,b_j}(\mathrm{x})\mathbf{H}_{,\mathrm{X}}(\mathbf{x}) + \mathbf{A}^{-1}(\mathbf{x})\mathbf{H}_{,\mathrm{X}b_j}(\mathbf{x})\end{pmatrix}\end{aligned} \tag{43}$$

Where

$$\begin{aligned}\mathbf{A}^{-1}_{,\mathrm{X}b_j}(\mathbf{x}) = &-\mathbf{A}^{-1}_{,b_j}\mathbf{A}_{,\mathrm{X}}\mathbf{A}^{-1} - \mathbf{A}^{-1}\mathbf{A}_{,\mathrm{X}b_j}\mathbf{A}^{-1} \\ &- \mathbf{A}^{-1}\mathbf{A}_{,\mathrm{X}}\mathbf{A}^{-1}_{,b_j}\end{aligned} \tag{44}$$

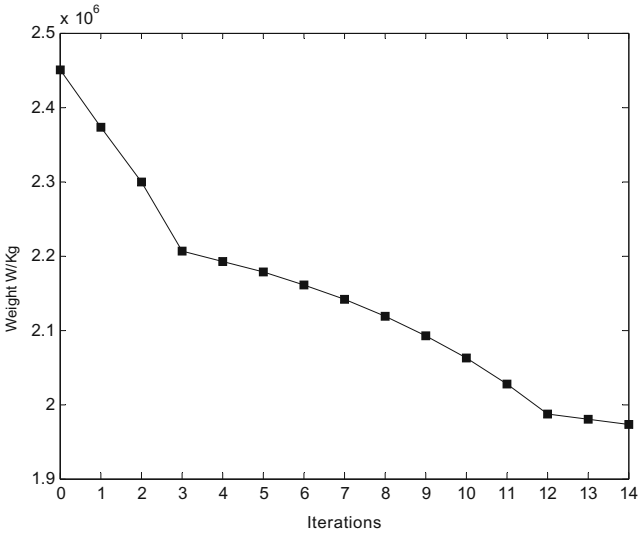

Fig. 6 Weight reduction history of the arc

$$\begin{aligned}\mathbf{A}_{,\mathrm{X}b_j}(\mathbf{x}) = \sum_{I=1}^{IP} \big(&\omega_{,\mathrm{X}b_j}(\mathbf{x}_I-\mathbf{x})\mathbf{p}(\mathbf{x}_I-\mathbf{x})\mathbf{p}^{\mathrm{T}}(\mathbf{x}_I-\mathbf{x})\\ &+\omega_{,\mathrm{X}}(\mathbf{x}_I-\mathbf{x})\mathbf{p}_{,b_j}(\mathbf{x}_I-\mathbf{x})\mathbf{p}^{\mathrm{T}}(\mathbf{x}_I-\mathbf{x})\\ &+\omega_{,\mathrm{X}}(\mathbf{x}_I-\mathbf{x})\mathbf{p}(\mathbf{x}_I-\mathbf{x})\mathbf{p}^{\mathrm{T}}_{,b_j}(\mathbf{x}_I-\mathbf{x})\\ &+\omega_{,b_j}(\mathbf{x}_I-\mathrm{x})\mathbf{p}_{,\mathrm{X}}(\mathbf{x}_I-\mathbf{x})\mathbf{p}^{\mathrm{T}}(\mathbf{x}_I-\mathbf{x})\\ &+\omega(\mathbf{x}_I-\mathbf{x})\mathbf{p}_{,\mathrm{X}}(\mathbf{x}_I-\mathbf{x})\mathbf{p}^{\mathrm{T}}_{,b_j}(\mathbf{x}_I-\mathbf{x})\\ &+\omega_{,b_j}(\mathbf{x}_I-\mathbf{x})\mathbf{p}(\mathbf{x}_I-\mathbf{x})\mathbf{p}^{\mathrm{T}}_{,\mathrm{X}}(\mathbf{x}_I-\mathbf{x}))\\ &+\omega(\mathbf{x}_I-\mathbf{x})\mathbf{p}_{,b_j}(\mathbf{x}_I-\mathbf{x})\mathbf{p}^{\mathrm{T}}_{,\mathrm{X}}(\mathbf{x}_I-\mathbf{x}))\end{aligned} \tag{45}$$

$$\begin{aligned}\mathbf{H}_{,\mathrm{X}b_j}(\mathbf{x}) = [&\mathbf{p}_{,\mathrm{x}}(\mathbf{x}_1-\mathbf{x})\omega_{,b_j}(\mathbf{x}_1-\mathbf{x})+\mathbf{p}_{,b_j}(\mathbf{x}_1-\mathbf{x})\omega_{,}(\mathbf{x}_1-\mathbf{x})\\ &+\mathbf{p}(\mathbf{x}_1-\mathbf{x})\omega_{,\mathrm{X}b_j}(\mathbf{x}_1-\mathbf{x}),\ \mathbf{p}_{,\mathrm{x}}(\mathbf{x}_2-\mathbf{x})\omega_{,b_j}(\mathbf{x}_2-\mathbf{x})\\ &+\mathbf{p}_{,b_j}(\mathbf{x}_2-\mathbf{x})\omega_{,\mathrm{x}}(\mathbf{x}_2-\mathbf{x})+\mathbf{p}(\mathbf{x}_2-\mathbf{x})\omega_{,\mathrm{X}b_j}(\mathbf{x}_2-\mathbf{x}),\\ &\cdots,\ \mathbf{p}_{,x}(\mathbf{x}_1-\mathbf{x})\omega_{,b_j}(\mathbf{x}_I-\mathbf{x})+\mathbf{p}_{,b_j}(\mathbf{x}_I-\mathbf{x})\omega_{,x}(\mathbf{x}_I-\mathbf{x})\\ &+\mathbf{p}(\mathbf{x}_I-\mathbf{x})\omega_{,\mathrm{X}b_j}(\mathbf{x}_I-\mathbf{x})]\end{aligned} \tag{46}$$

In SAM, the design derivatives $\Phi_{,b_j}(\mathbf{x})$ and $\Phi_{,Xb_j}(\mathbf{x})$ are solved by using FDM. The perturbation step size of design variable is defined as Δb which is very small and determines the calculating precision. The acceptable results can be obtained when Δb is in the range of $10^{-2}\sim10^{-5}$ (Bakshi and Pandey 2000). In this paper, suppose that Δb= 0.001, then $\Phi_{,b_j}(\mathbf{x})$ and $\Phi_{,Xb_j}(\mathbf{x})$ are approximated by

$$\Phi_{,b_j}(\mathbf{x}) \approx \frac{\Phi\big(\mathbf{x},\mathbf{b}+\Delta b\mathbf{I}_j\big)-\Phi(\mathbf{x},\mathbf{b})}{\Delta b} \tag{47}$$

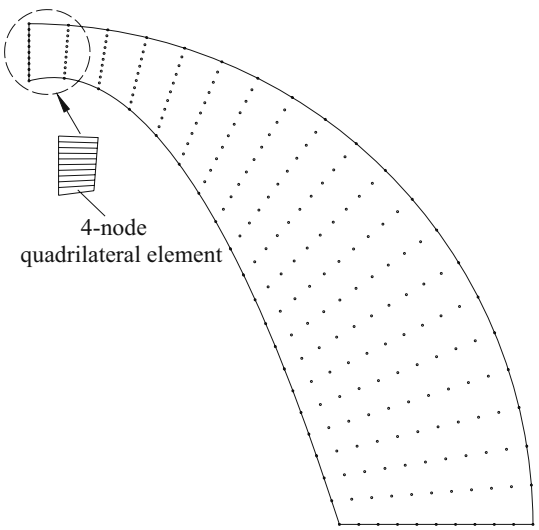

Fig. 7 Optimum shape of the arc

Table 5 Comparison of the natural frequency of the arc (unit: hertz)

Modal	1	2	3	4	5
Initial natural frequencies	14.105	41.877	59.904	84.923	112.45
Optimum natural frequencies	8.6080	36.278	49.902	78.606	88.728

$$\Phi_{,\mathrm{X}b_j}(\mathbf{x}) \approx \frac{\Phi_{,\mathrm{X}}\big(\mathbf{x},\mathbf{b}+\Delta b\mathbf{I}_j\big)-\Phi_{,\mathrm{X}}(\mathbf{x},\mathbf{b})}{\Delta b} \tag{48}$$

Where $\mathbf{I}_j$ is the same dimension as the design variable vector $\mathbf{b}$, having unit value at the jth position and zeros elsewhere, and the subscript "$,\mathbf{x}b_j$" denotes the second-order partial derivative $\partial^2/\partial\mathbf{X}\partial b_j$, namely, $\partial^2/\partial x\partial b_j$ or $\partial^2/\partial y\partial b_j$ in 2D.

5 Numerical examples

5.1 Dynamic sensitivity analysis of a cantilever beam

The cantilever beam, as shown in Fig. 1, is discretized uniformly by 153 particles and analyzed. The material properties of the beam are: Young's modulus E=300 MPa, Poisson's ratio μ=0.3, thickness th=1 m, density ρ=1.0 kg/m^3. The beam without damp subjected to an impact concentrated load F at the free end. F=1,000 N, as shown in Fig. 2, and the impact time t=0.5 s. In this paper, a time step Δt=0.002 s is used in *Wilson-θ* method.

In the process of dynamic sensitivity analysis, the width H is selected as the design variable, and supposing that $\mathbf{V}(\mathbf{x})$ is a linear design velocity field as follows

$$V_x(\mathbf{x}) = 0 \tag{49}$$

$$V_y(\mathbf{x}) = \frac{6-y}{H} \tag{50}$$

We obtain the results shown in Table 1 for the first five natural frequencies and Table 2 for the sensitivities of the first five natural frequencies. In addition, comparisons for displacement response u_y and displacement response sensitivity $u_{y,b}$ of the free end (at B point) of the beam are presented in Figs. 3 and 4 separately.

5.2 Natural frequency sensitivity and shape optimization of an arc

The arc is studied generally in static optimization problems (Pourazady and Fu 1996). In this paper, an arc shown in Fig. 5 is discretized by 231 uniformed particles and analyzed. The material properties of the arc are: Young's modulus E=2.07e5 MPa, Poisson's ratio μ=0.3, thickness th=1 m, and density ρ=7,800 kg/m^3.

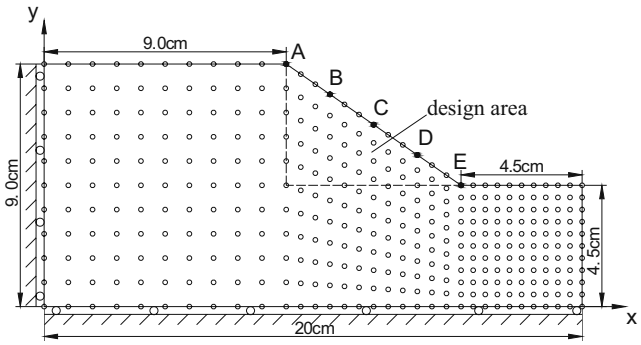

Fig. 8 Node distribution of the fillet

In the frequency sensitivity analysis, we consider the inner radius r_1 as the design variable, and suppose that $\mathbf{V}(\mathbf{x})$ is a linear design velocity field as follows

$$V_x(\mathbf{x}) = \frac{r_2 \cos\theta - x}{r_2 - r_1} \tag{51}$$

$$V_y(\mathbf{x}) = \frac{r_2 \sin\theta - y}{r_2 - r_1} \tag{52}$$

The results obtained are shown in Table 3 for the first five inherent frequencies and Table 4 for their sensitivities, respectively.

The objective function is the weight of the arc, and the behavior constraint is the first natural frequency. The shape of the inner arc AC is represented by a quadratic polynomial which is determined by three key points $A\left(r_A \cos\frac{\pi}{2}, r_A \sin\frac{\pi}{2}\right)$, $B\left(r_B \cos\frac{\pi}{4}, r_B \sin\frac{\pi}{4}\right)$ and C($r_C$cos0, $r_C$sin0), and the optimization model is shown as

$$\min W(\mathbf{b}) \tag{53}$$

$$s.t. \begin{cases} \omega_1 \geq 8.5\text{Hz} \\ 15\text{m} \leq r_A \leq 23\text{m} \\ 15\text{m} \leq r_B \leq 16\text{m} \\ 15\text{m} \leq r_C \leq 18\text{m} \end{cases}$$

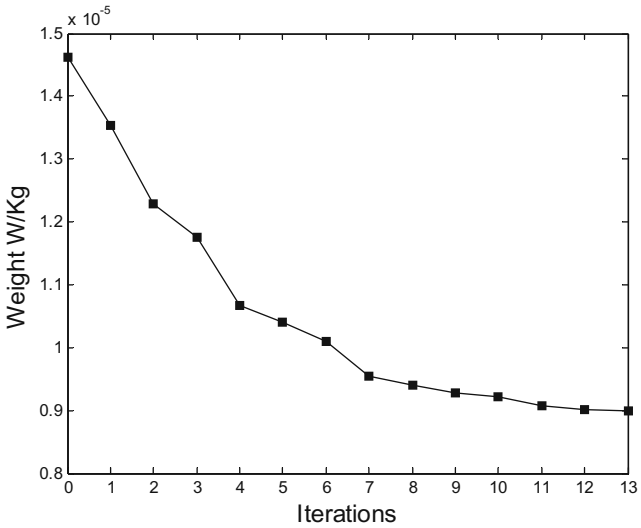

Fig. 9 Weight reduction history of the fillet

The solution of this problem has converged after 14 design iterations, and the total weight of the arc is reduced by 19.5%, as shown in Fig. 6. The optimum shape and inherent frequencies are presented in Fig. 7 and Table 5, respectively.

5.3 Dynamic shape optimization of a fillet

The fillet shown in Fig. 8 is a classical geometric model in static shape optimization problems (Phan et al. 1998). In this paper, the shape optimization of the fillet is performed mostly in the perspective of dynamic property. The material constants are: Young's modulus E=10 MPa, Poisson's ratio μ=0.3, thickness th=1 cm, and density ρ=1.0 kg/m^3.

The domain of the fillet is discretized by 363 particles, and 11 of them are equally spaced on the design boundary AE that is represented by a piecewise spline curve which is controlled by five key points A(9.0, 9.0), B(10.625, y_B), C(12.25, y_C), D(13.875, y_D), and E(15.5, 4.5). Presuming that the spline function satisfies the nature boundary condition at endpoint, the y coordinates of points B, C, and D on the design boundary are selected as the design variables, and the points A and E remain fixed during the shape optimization.

The optimal objective is to find the optimum shape of the fillet that minimizes the weight of the design area under the first natural frequency constraints, and the optimization model is shown as

$$\min W(\mathbf{b}) \tag{54}$$

$$\text{s.t.} \begin{cases} 4,465\text{Hz} \leq \omega_1 \leq 4,500\text{Hz} \\ 6.7\text{cm} \leq y_B \leq 9.0\text{cm} \\ 5.5\text{cm} \leq y_C \leq 9.0\text{cm} \\ 4.8\text{cm} \leq y_D \leq 9.0\text{cm} \end{cases}$$

The optimum design is obtained after 13 iterations, and the weight of the design area is reduced by 38.5%, as

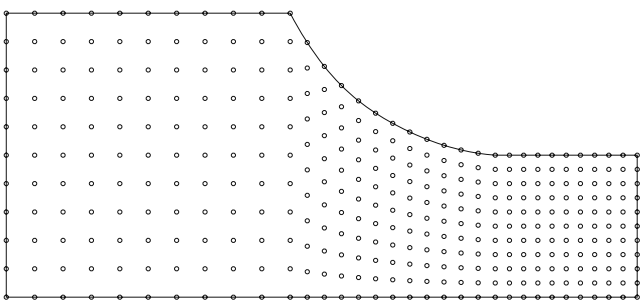

Fig. 10 Optimum shape of the fillet

Table 6 Comparison of the natural frequency of the fillet (unit: hertz)

Modal	1	2	3	4	5
Initial natural frequencies	4,463.18	9,046.68	10,054.7	11,348.9	13,713.9
Optimum natural frequencies	4,478.77	9,095.55	10,409.6	11,185.3	14,105.0

shown in Fig. 9. The final shape and natural frequencies of the fillet are presented in Fig. 10 and Table 6 separately.

By means of these numerical examples, we have demonstrated that the dynamic sensitivity analysis method proposed in this paper is valid and efficient. In dynamic analysis, the results obtained by the present RKPM are in very good agreement with those obtained using FEM, and the small differences are probably caused by the fact that the radius of influential domain d_m, the penalty factor α, and the size of the time step Δt affect the computational results more or less. In dynamic sensitivity analysis, the sensitivities of the natural frequency and displacement response obtained by DDM based on RKPM and those obtained using SAM and GFM based on RKPM match well, and the errors were due to the effects of the perturbation step size for design variable in the latter.

In the meanwhile, the advantage that the RKPM shape function needs no element or mesh is presented in the process of dynamic shape optimization. The mesh distortion would exist if the FEM were used during the shape optimization, as shown in Fig. 6, the length–width ratios of the four-node quadrilateral elements would be so high at the left end of the arc that the computational accuracy was influenced badly. As for the fillet, the mesh distortion in Gong et al. (2006a, b) would similarly exist if the FEM were used in dynamic shape optimization.

6 Conclusions

By means of the numerical analysis and discussion, we draw some conclusions as follows

- The RKPM based on node approximation is used to carry out the structural dynamic shape optimization, and in the process of optimization, the mesh distortion of finite element can be eliminated completely and without requiring remeshing. That's just the unparalleled superiority over traditional FEM, and a new numerical method is provided for structural dynamic optimization design.
- The discrete natural frequency sensitivity equation and dynamic response sensitivity equation based on RKPM are proposed by using DDM. It is shown that the present method is valid and very easy to implement. The computational results are in very good agreement with those obtained using FEM, SAM, or GFDM.
- The significant difference between the FEM and RKPM is that the design derivative of the RKMP shape function is nonzero when the structural natural frequency and dynamic response sensitivity analysis are performed.

The RKPM can also be easily generalized to the sensitivity analysis of dynamic problem of other structures, such as plates, shells, and 3D structures. It is of great practical significance to perform dynamic sensitivity analysis and shape optimization using RKPM. However, as a new numerical method, RKPM is not better than FEM in imposing the boundary condition, the improvement of the computational efficiency, the extension for application scope, and the development of business software now. These are subjects for further investigation.

Acknowledgments This research is supported by National Natural Science of China under Grant Number 50475143.

References

Bakshi P, Pandey PC (2000) Semi-analytical sensitivity using hybrid finite elements. Comput Struct 77(2):201–213

Bobaru F, Mukherjee S (2001) Shape sensitivity analysis and shape optimization in planar elasticity using the element-free Galerkin method. Comput Methods Appl Mech Eng 190:4319–4337

Bogomolni M, Kirsch U, Sheinman I (2006) Efficient design sensitivities of structures subjected to dynamic loading. Int J Solids Struct 43(18–19):5485–5500

Falco SA, Afonso SMB, Vaz LE (2004a) Analysis and optimal design of plates and shells under dynamic loads-I: finite element and sensitivity analysis. Struct Multidiscipl Optim 27(3):189–196

Falco SA, Afonso SMB, Vaz LE (2004b) Analysis and optimal design of plates and shells under dynamic loads-II: optimization. Struct Multidiscipl Optim 27(3):197–209

Francavilla A, Ramakrishnan CV, Zienkiewicz OC (1975) Optimization of shape to minimize stress concentration. J Strain Anal 10 (2):63–70

Gong SG, Chen YP, Huang YQ (2006a) Application research of meshless method in shape optimization. China Mech Eng 17(12):1290–1294 (In Chinese)

Gong SG, Chen YP, Huang YQ et al (2006b) Shape optimization and sensitivity analysis based on element-free galerkin methods. Chin J Mech Eng 42(6):199–204 (In Chinese)

Grandhi R (1993) Structural optimization with frequency constraints-a review. AIAA J 31(12):2296–2303

Grindeanu I, Choi KK, Chen JS et al (1999) Shape design optimization of hyperelastic structures using a meshless method. AIAA J 37(8):990–997

Gu SN, Xu B, Rong JH et al (2005) Recent progresses on structural dynamic design methods. J Mech Strength 27(2):156–162 (In Chinese)

Keulen FV, Haftka RT, Kim NH (2005) Review of option for structural design sensitivity analysis part I: linear system. Comput Methods Appl Mech Eng 194:3213–3243

Kim NH, Choi KK (2001) Design sensitivity analysis and optimization of nonlinear transient dynamics. Mechan Struct Mach 29(3):351–371

Kim NH, Choi KK, Chen JS et al (2000) Meshless shape design sensitivity analysis and optimization for contact problem with friction. Comput Mech 25:157–168

Kim NH, Choi KK, Botkin ME (2003) Numerical method for shape optimization using meshfree method. Struct Multidiscipl Optim 24:418–429

Liao BY, Zhou XM, Yin ZH (2003) Modern mechanical dynamics and its engineering application-modeling, analysis, simulation, control, modification and optimization. China Machine Press, Beijing (Chinese version)

Liu WK, Jun S, Zhang YF (1995) Reproducing kernel particle methods. Int J Numer Methods Eng 20:1081–1106

Phan AV, Mukherjee S, Mayer JR (1998) Stress, stress sensitivity and shape optimization in two-dimensional linear elasticity by the boundary contour method. Int J Numer Methods Eng 42:1391–1407

Pourazady M, Fu Z (1996) An integrated approach to structural shape optimization. Comput Struct 60(2):279–289

Rong JH, Zheng JL, Xu FH (2002) Structural dynamic modification and optimization design. China Communications Press, Beijing (Chinese version)

Yoo HH, Cho JE, Chung JT (2006) Modal analysis and shape optimization of rotating cantilever beams. J Sound Vib 290:223–241

Zhang ZQ, Zhou JX, Zhou N et al (2005) Shape optimization using reproducing kernel particle method and an enriched genetic algorithm. Comput Methods Appl Mech Eng 194:4048–4070

Zhou JX, Wang XM, Zhang ZQ et al (2005a) On the enhancement of computation and exploration of discretization approaches for meshless shape design sensitivity analysis. Struct Multidiscipl Optim 31:96–104

Zhou JX, Zhang HY, Zhang L (2005b) Reproducing kernel particle method for free and forced vibration analysis. J Sound Vib 279:389–402